rected pTAC as an input function. We assumed that free and non-specifically bound ligands are present in a rapid equilibrium state. Therefore, in the metabolite analysis the plasma was treated with TCA in acetonitril solution to recover quantitatively both free and non-specifically bound radioactivities.

4.2. Distribution volume in the brain

As shown in Table 1, DV values of [^{11}C]DOX in the temporal, frontal and cingulate cortices were larger than that in the occipital cortex in this study. The DV of [^{11}C]DOX reflecting both specific and non-specific binding in these cortical regions, was proportional well to the H1R density measured in vitro by using [^{3}H]doxepin (Fig. 4). Because the cerebellar H1R density was negligibly low compared to the cortical densities in the post-mortem brain studies [5,14,30], the DV in the cerebellum is reasonably assumed to be the free and non-specific bound pool of [^{11}C]DOX in the brain. Thus, the specific DV reflecting the specific binding of [^{11}C]DOX in the cortical regions can be evaluated by subtracting the DV in the cerebellum from those in the cortical regions. On the other hand, DVs in the thalamus, caudate nucleus and putamen were similar to those in the cortices, though the H1R densities in the subcortical region were lower than those in the cortices in post-mortem studies [5,14,29] (Table 1). The correlation between the DVs and the reported H1R densities in all subcortical brain regions deviated significantly from the expected values compared to those in the cortices, suggesting that DVs in the thalamus and the striatum would not reflect the H1R densities exactly. We estimated DV in each brain region with tTAC obtained by the ROI placed on the gray matter referencing to the MRI image of each subject. Thus, the ROI placement would not be a cause of the discrepancy between the present in vivo and the previous in vitro studies. The competition between [^{11}C]DOX and endogenous histamine would be almost same in the brain, since projection of histaminergic neurons is almost uniform in the brain. One reason for the discrepancy could be the higher non-specific binding in the thalamus and striatum [18]. Yanai et al. measured specific binding and non-specific binding with the autopsied human brain using [^{3}H]pyrilamine. They found that non-specific binding in the thalamus and the striatum was 212% and 125% of the cortex, respectively [30]. We also confirmed that these regions showed the higher non-specific binding of [^{11}C]DOX than the cortical regions by the blocking study with d-chlorpheniramine [31]. In the in vitro ligand-receptor binding studies, the H1R density was defined as the radioactivity specifically bound after subtracting the non-specific binding determined in the presence of a large amount of antihistaminic drug [5,14,30], while the specific DVs were determined by subtracting the DV in the cerebellum from that in each region. The subtraction would not be able to eliminate properly the binding sites except for H1Rs in the thalamus, caudate nucleus and putamen.

In this paper, it was found that a two-compartment model is suitable for quantitative PET measurement of H1Rs using [^{11}C]DOX and a non-linear curve fitting. The [^{11}C]DOX and PET gives reliable information on the H1Rs in cortical regions because it has limited potential in subcortical regions such as the striatum and thalamus, possibly because of nonspecific binding [24].

Acknowledgments

This work was partly supported by Grants-in-Aid from the Ministry of Education, Culture, Sports, Science, and Technology, and from the Ministry of Health, Labor and Welfare, Japan. The authors thank the volunteers in the PET measurement, Ms. Miyoko Ando for care of subjects and Mr. Kazunori Kawamura for the preparation of [^{11}C]DOX.

References

[1] Adelberg BR. Sedation and performance issues in the treatment of allergic conditions. Arch Int Med 1997;157:494–500.
[2] Akaike H. A new look at the statistical model identification. IEEE Automatic Control A 1974;C19:716–22.
[3] Borse GJ. Numerical Methods with MATLAB. International Stamford: Thomson Publishing Inc.; 1997, p. 177-188.
[4] Bressan RA, Erlandsson K, Jones HM, Mulligan RS, Ell PJ, Pilowsky LS. Optimizing limbic selective D2/D3 receptor occupancy by risperidone: a [^{123} I]-epidepride SPET study. J Clin Psychopharmacol 2003;23(1):5–14.
[5] Chang RSL, Tran VT, Snyder SH. Heterogeneity of histamine H1-receptors: Specific variations in [^{3}H]mepyramine binding of brain membranes. J Neurochem 1979;32:1653–63.
[6] Chugani DC, Muzik O, Chakraborty P, Mangner T, Chugani HT. Human brain serotonin synthesis capacity measured in vivo with alpha-[C-11]methyl-L-tryptophan. Synapse 1998;28(1):33–43.
[7] DaSilva JN, Lourenco CM, Meyer JH, Hussey D, Potter WZ, Houle S. Imaging cAMP-specific phosphodiesterase-4 in human brain with R-[^{11} C]rolipram and positron emission tomography. Eur J Nucl Med Mol Imaging 2002;29(12):1680–3.
[8] Haas H, Panula P. The role of histamine and the tuberomamillary nucleus in the nervous system. Nat Rev Neurosci 2003;4(2):121–30.
[9] Hagberg GE, Torstenson R, Marteinsdottir I, Fredrikson M, Langstrom B, Blomqvist G. Kinetic compartment modeling of [^{11}C]-5-hydroxy-L-tryptophan for positron emission tomography assessment of serotonin synthesis in human brain. J Cereb Blood Flow Metab 2002;22(11):1352–66.
[10] Higuchi M, Yanai K, Okamura N, Meguro K, Arai H, Itoh M, Iwata R, Ido T, Watanabe T, sasaki H. Histamine H_1 receptors in patients with Alzheimer's disease assessed by positron emission tomography. Neuroscience 2000;99:721–9.
[11] Iwata R, Pascali C, Bogni A, Yanai K, Kato M, Ido T, Ishiwata K. A combined loop-SPE method for the automated preparation of [^{11}C]doxepin. J Label Compd Radiopharm 2002;45:271–80.
[12] Ishiwata K, Koyanagi Y, Saitoh T, Taguchi K, Toda J, Sano T, Senda M. Effects of single and repeated administration of 1,2,3,4-tetrahydroisoquinoline analogs on the binding of [^{11}C]raclopride to dopamine D_2 receptors in the mouse brain. J Neural Transm 2001;108: 1111–25.
[13] Ishiwata K, Itou T, Ohyama M, Yamada T, Mishina M, Ishii K, Nariai T, Sasaki T, Oda K, toyama H, Senda M. Metabolite analysis

of [^{11}C]flumazenil in human plasma: assessment as the standardized value for quantitative PET studies. Ann Nucl Med 1998;12:55–9.

[14] Kanba S, Richelson E. Histamine H_1 receptors in human brain labeled with [^{3} H]doxepin. Brain Res 1984;304:1–7.

[15] Kane GC, Lipsky JJ. Drug-grapefruit juice interactions. Mayo Clin Proc 2000;75:933–42.

[16] Koeppe RA, Holthoff VA, Frey KA, Kilbourn MR, Kuhl DE. Compartmental analysis of [^{11}C]flumazenil kinetics for the estimation of ligand transport rate and receptor distribution using positron emission tomography. J Cereb Blood Flow Metab 1991;11:735–44.

[17] Lopez-Garcia JA, Ramis C, Nicolau MC, alemany G, Planas B, Rial R. Histaminergic drugs in the rat caudate nucleus: effects on learned helplessness. Pharmacol Biochem Behav 1993;45(2):275–82.

[18] Martinez-Mir MI, Pollard H, Moreau J, Arrang JM, Ruat M, Traiffort E, Schwartz JC, Palacios JM. Three histamine receptors (H1, H2 and H3) visualized in the brain of human and non-human primates. Brain Res 1990;526(2):322–7.

[19] Mintun MA, Raichle ME, Kilbourn MR, Wooten GF, Welch MJ. A quantitative model for the in vivo assessment of drug binding sites with positron emission tomography. Ann Neurol 1984;15:217–227.

[20] Mochizuki H, Tashiro M, Tagawa M, Kano M, Itoh M, Okamura N, Watanabe T, Yanai K. The effects of a sedative antihistamine, d-chlorpheniramine, on visuomotor spatial discrimination and regional brain activity as measured by positron emission tomography (PET). Hum Psychopharmacol 2002;17(8):413–8.

[21] Moscati RM, Moore GP. Comparison of cimetidine and diphenhydramine in the treatment of acute urticaria. Ann Emerg Med 1990; 19(1):12–5.

[22] Nicholson AN. Central effects of H1 and H2 antihistamines. Aviat Space Environ Med 1985;56:293–8.

[23] Parmentier R, Ohtsu H, Djebbara-Hannas Z, Valatx JL, Watanabe T, Lin JS. Anatomical, physiological, and pharmacological characteristics of histidine decarboxylase knock-out mice: evidence for the role of brain histamine in behavioral and sleep-wake control. J Neurosci 2002;22(17):7695–711.

[24] Schmitt GJ, Meisenzahl EM, Dresel S, tatsch K, Rossmuller B, Frodl T, Preuss UW, Hahn K, Moller HJ. Striatal dopamine D2 receptor binding of risperidone in schizophrenic patients as assessed by 123I-iodobenzamide SPECT: a comparative study with olanzapine. J Psychopharmacol 2002;16(3):200–6.

[25] Szabo Z, McCann UD, Wilson AA, Scheffel U, Owonikoko T, Mathews WB, Ravert HT, Hilton J, Dannals RF, Ricaurte GA. Comparison of (+)-^{11} C-McN5652 and ^{11} C-DASB as serotonin transporter radioligands under various experimental conditions. J Nucl Med 2002;43(5):678–92.

[26] Tagawa M, Kano M, Okamura N, Higuchi M, Matsuda M, Mizuki Y, Arai H, Iwata R, Fujii T, Komemushi S, Ido T, Itoh M, Sasaki H, Watanabe T, Yanai K. Neuroimaging of histamine H1-receptor occupancy in human brain by positron emission tomography (PET): a comparative study of ebastine, a second-generation antihistamine, and (+)-chlorpheniramine, a classical antihistamine. Br J Clin Pharmacol 2001;2:501–509.

[27] Watanabe T, Taguchi Y, Shiosaka S, Tanaka J, Kubota H, Terano Y, Tohyama M, Wada H. Distribution of histaminergic neuron system in the central nervous system of rats; a fluorescent immunohistochemical analysis with histidine decarboxylase as a marker. Brain Res 1984;295:13–25.

[28] Watanabe T, Yanai K. Studies on functional roles of the histaminergic neuron system by using pharmacological agents, knockout mice and positron emission tomography. Tohoku J Exp Med 2001;195: 197–217.

[29] Yanai K, Watanabe T, Yokoyama H, Hatazawa J, Iwata R, Ishiwata K, Meguro K, Itoh M, Takahashi T, Ido T. Mapping of histamine H_1 receptors in the human brain using [^{11}C]pyrilamine and positron emission tomography. J Neurochem 1992;59:128–36.

[30] Yanai K, Watanabe T, Meguro K, Yokoyama H, Sato I, Sasano H, Itoh M, Iwata R, Takahashi T, Ido T. Age-dependent decrease in histamine H_1 receptor in human brains revealed by PET. Neuroreport 1992;3(5):433–6.

[31] Yanai K, Watanabe T, Yokoyama H, Meguro K, Hatazawa J, Itoh M, Iwata R, Ishiwata K, Takahashi T, Ido T. Histamine H_1 receptors in human brain visualized in vivo by [^{11} C]doxepin and positron emission tomography. Neurosci Lett 1992;137:1457.

ELSEVIER

Nuclear Medicine and Biology 31 (2004) 165–171

NUCLEAR MEDICINE — AND — BIOLOGY

www.elsevier.com/locate/nucmedbio

Quantitative measurement of histamine H_1 receptors in human brains by PET and [^{11}C]doxepin

Hideki Mochizuki[a,b], Yuichi Kimura[b,*], Kenji Ishii[b], Keiichi Oda[b], Toru Sasaki[b], Manabu Tashiro[a], Kazuhiko Yanai[a], Kiichi Ishiwata[b]

[a]*Department of Pharmacology, Tohoku University School of Medicine, Sendai, Japan*
[b]*Positron Medical Center, Tokyo Metropolitan Institute of Gerontology, Tokyo, Japan*

Received 11 May 2003; received in revised form 4 August 2003; accepted 30 August 2003

Abstract

The aim of this study is to establish a method for quantitative measurement of histamine H_1 receptor (H1R) in human brain by PET and [^{11}C]doxepin ([^{11}C]DOX). The estimated parameters with a two-compartment model were stable for the initial values for parameter estimation but those with a three-compartment model were not. This finding suggests that the H1R measured by the [^{11}C]DOX and PET can be evaluated with a two-compartment model. © 2004 Elsevier Inc. All rights reserved.

Keywords: Compartment model; Histamine H_1 receptor; PET; [^{11}C]doxepin

1. Introduction

Histamine neurons are exclusively located in the tuberomammillary nucleus of hypothalamus, and diffusely project their fibers to almost all areas of brain. They are thought to be involved in the regulation of various physiological functions such as wakefulness and cognition through at least four histamine receptor subtypes: G protein coupled H_1 ($G_{q/11}$), H_2 (G_s), H_3 (G_i) and H_4 (G_i) [8,23,27,28]. H_1 and H_2 receptors are located at the postsynaptic sites of the histamine neurons, and H_3 receptors are functioning as an autoreceptor. H_3 receptor-activation inhibits the release of neural histamine. It was reported that impairments of cognition and motor functions and sedation were caused by H_1 antagonists [8]. Histamine H_1 receptors (H1R) are important for cortical activation as well as H_2 receptors [17,21]. The precise functions of H_4 receptor in brains have been scarcely understood since it was found recently. Antihistaminic drugs are often used to relieve allergies, coughs and colds, but they elicit sedation and affect cognition and behavior through the cortical inactivation [1,20,22]. Therefore, many studies have been carried out to develop antihistaminic drugs that do not penetrate the blood brain barrier (BBB). The blockade of H1Rs in brains is cause of sedation. Therefore, it is important to evaluate the occupancy of H1Rs by antihistamine in order to verify the side effects of antihistaminic drugs on the central nervous system (CNS). In vivo imaging techniques such as single photon emission computed tomography (SPECT) and positron emission tomography (PET) can provide a clear understanding of physiological processes in the human brain. Therefore, the therapeutic efficacies of drugs on the CNS have been extensively investigated in term of the receptor occupancy in the living human brain [4,24]. As for the H1R occupancy by antihistaminic drugs, PET with [^{11}C]doxepin ([^{11}C]DOX) has been used to evaluate objectively their possible side effects due to the penetration through BBB [26].

For quantitative PET measurement of receptor density, an appropriate model to describe the underlying kinetic of the individual radioligand should be developed because the model is different among the ligands used, even though their target receptor is the same [6,9]. Most of receptor imaging studies underwent the compartment model analysis with a nonlinear curve fitting algorithm to evaluate receptor density [7,9]. So far the evaluation of H1R density by [^{11}C]DOX and PET was performed by usually established methods such a graphical analysis with a three-compartment

* Corresponding author. Tel.: +81-3-3964-3241 ex.3506; fax: +81-3-3964-2188.
E-mail address: ukimura@ieee.org (Y. Kimura).

doi:10.1016/j.nucmedbio.2003.08.010

Adenosine A_1 Receptor Mapping of the Human Brain by PET with 8-Dicyclopropylmethyl-1-^{11}C-Methyl-3-Propylxanthine

Nobuyoshi Fukumitsu, MD[1,2]; Kenji Ishii, MD[1]; Yuichi Kimura, PhD[1]; Keiichi Oda, PhD[1]; Toru Sasaki, PhD[1]; Yutaka Mori, MD, PhD[3]; and Kiichi Ishiwata, PhD[1]

[1]Positron Medical Center, Tokyo Metropolitan Institute of Gerontology, Tokyo, Japan; [2]Proton Medical Research Center, University of Tsukuba, Ibaragi, Japan; and [3]Department of Radiology, Jikei University School of Medicine, Tokyo, Japan

Adenosine is an endogenous modulator of synaptic functions in the central nervous system. To investigate the physiologic and pathologic roles of the adenosine receptors in the human brain, PET is a powerful in vivo technique. In this study, we quantitatively evaluated the distribution of a major subtype A_1 adenosine receptor in the human brain by PET with a newly developed radioligand, 8-dicyclopropylmethyl-1-^{11}C-methyl-3-propylxanthine (^{11}C-MPDX). **Methods:** In 5 healthy volunteers, after PET measurement of the regional cerebral blood flow (rCBF) with ^{15}O-H_2O, a 60-min PET scan with ^{11}C-MPDX was performed. The distribution volume (DV) of ^{11}C-MPDX was quantitatively evaluated by Logan's graphical analysis. **Results:** ^{11}C-MPDX was taken up at a high level, reaching a peak at 2–2.5 min, followed by a rapid decrease. The unchanged form of ^{11}C-MPDX in plasma was 75% at 60 min after injection. The DV of ^{11}C-MPDX was large in the striatum and thalamus, moderate in the cerebral cortices and pons, and small in the cerebellum. The distribution pattern of ^{11}C-MPDX in the brain was coincident with that of adenosine A_1 receptors in vitro, reported previously, but discretely different from that of rCBF. **Conclusion:** ^{11}C-MPDX PET has the potential for mapping adenosine A_1 receptors in the human brain.

Key Words: 8-dicyclopropylmethyl-1-^{11}C-methyl-3-propylxanthine; adenosine A_1 receptor; brain; PET

J Nucl Med 2005; 46:32–37

Adenosine is present in large amounts in the mammalian brain and plays a role as an endogenous modulator of synaptic functions in the central nervous system. The effects are mediated by at least 4 adenosine receptor subtypes: A_1, A_{2A}, A_{2B}, and A_3. The 2 major subtypes of receptors—A_1 and A_2 receptors—have been investigated well in molecular biology, pharmacology, and physiology (*1–3*). The adenosine A_1 receptors exhibit a high affinity for adenosine and inhibit adenylyl cyclase. It is now known that A_1 receptors are G protein linked and can act through effectors other than adenylyl cyclase, including potassium channels, calcium channels, phospholipase A_2 and C, and guanylyl cyclase (*1*).

Previous work has established a role for adenosine in a diverse array of neural phenomena, which include regulation of sleep and the level of arousal, neuroprotection, regulation of seizure susceptibility, locomotor effects, analgesia, mediation of the effects of ethanol, and chronic drug use (*4*). They are mediated by both adenosine A_1 and A_{2A} receptors. Therefore, interaction with adenosine metabolism is a promising target for therapeutic intervention in ischemic brain disorders, neurologic and psychiatric diseases such as epilepsy, sleep, movement (parkinsonism or Huntington's disease), or psychiatric disorders (Alzheimer's disease, depression, schizophrenia, or addiction) (*3,5,6*).

For the purpose of mapping adenosine A_1 and A_{2A} receptors in the brain by PET, we synthesized and characterized several radioligands (*7,8*). Recently we performed imaging of adenosine A_1 receptors in the human brain by PET with 8-dicyclopropylmethyl-1-^{11}C-methyl-3-propylxanthine (^{11}C-MPDX) (Fig. 1) (*9*) following the developmental studies with animals (*7,10–15*). Bauer et al. also reported the mapping of adenosine A_1 receptors in the human brain by PET with a xanthine-type analog, 8-cyclopentyl-3-(3-^{18}F-fluoropropyl)-1-propylxanthine (^{18}F-CPFPX) (*16*). In this study, we quantitatively evaluated the distribution volume (DV) of ^{11}C-MPDX in the brain of healthy volunteers by a graphical analysis method.

MATERIALS AND METHODS

The study protocol was approved by the Institutional Ethical Committee. Five male volunteers (age, 21.6 ± 1.5 y old; age range, 20–24 y old; body weight, 62.4 ± 2.3 kg; body weight range, 59–64 kg) participated in this study, and written informed consent was obtained from the subjects. All subjects were healthy according to the history, physical, neurologic, and psychiatric examinations, and MRI study of the brain before the PET study.

Received Mar. 18, 2004; revision accepted Aug. 12, 2004.
For correspondence or reprints contact: Nobuyoshi Fukumitsu, MD, Proton Medical Research Center, University of Tsukuba, 1-1-1, Tennoudai, Ibaragi, 305-8575, Japan.
E-mail: GZL13162@nifty.ne.jp

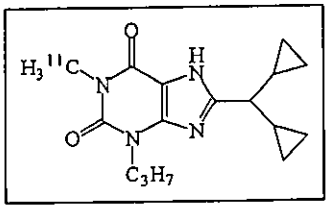

FIGURE 1. Chemical structure of ^{11}C-MPDX.

Radiosynthesis of ^{11}C-MPDX was performed as previously described (*10,14*). The injection radioactivity dose was 611 ± 93 MBq (range, 484–700 MBq), and the mass was 15.5 ± 6.9 nmol (range, 9.9–27.5 nmol). The specific radioactivity was 43.4 ± 13.4 TBq/mmol (range, 25.5–55.6 TBq/mmol).

PET Measurement

PET measurement was performed with a SET-2400W (Shimadzu Co.), which acquires 63 slices having 128 ×128 pixels each at a transverse resolution of 4.5-mm full width of half maximum (FWHM) and at an axial resolution of 5.8-mm FWHM. Scanning took place as the subjects laid supine. A venous catheter was inserted into a forearm vein of the subjects for tracer injection, and an arterial catheter was inserted into a distal radial artery under local anesthesia for sampling arterial blood. After positioning the subject's head in the canthomeatal orientation, a transmission scan was performed with a rotating ^{68}Ga/^{68}Ge line source to correct for the photon attenuation using the attenuation map. Then, ^{15}O-H_2O (120–150 MBq) was injected intravenously into the subject for a period of 10 s, and a PET scan was performed for 120 s in a 3-dimensional static mode. Ten minutes later, after the first scan, the subject was given ^{11}C-MPDX for a period of 10 s, and the second PET scan was performed for 60 min in a 2-dimensional dynamic mode (10 s × 6 frames, 30 s × 3 frames, 60 s × 5 frames, 150 s × 5 frames, and 300 s × 8 frames). The tomographic images were reconstructed using a filtered backprojection method and Butterworth filter (cutoff frequency, 1.25 cycle/cm; order, 2). The data were collected in a 128 × 128 × 31 matrix. The voxel size was 2 × 2 × 6.25 mm.

Blood Sampling and Metabolite Analysis

Arterial blood was taken at 10, 20, 30, 40, 50, 60 70, 80, 90, 100, 110, 120, 135, and 150 s and at 3, 5, 7, 10, 15, 20, 30, 40, 50, and 60 min. The whole blood and plasma were measured for radioactivity with a γ-counter and weighed. The time–activity curves were expressed as becquerels per milliliter or the standardized uptake value (SUV) (grams body weight × Bq/mL tissue/total injected dose). The unchanged form of ^{11}C-MPDX in the plasma sampled at 3, 10, 20, 30, 40, and 60 min was analyzed by high-performance liquid chromatography (HPLC) as described (*10*).

Kinetic Analysis

PET images were registrated and resliced to MRI with the Ardekani image registration algorithm (*17*) by UNIX workstations (Silicon Graphics Inc.) using the Dr. View image analysis software system (Asahi Kasei Joho System). Regions of interest (ROIs) were placed on the frontal, medial frontal, temporal, medial temporal, parietal, and occipital cortices, striatum, thalamus, cerebellum, and pons based on MRI. The ROI in the frontal cortex had 835 voxels and that in the pons had 87 voxels (1 pixel = 2 × 2 × 6.25 mm). The pixel numbers in other regions were in-between. The regional cerebral blood flow (rCBF) was measured by the autoradiographic method (*18*). The binding of ^{11}C-MPDX was evaluated by a graphical analysis according to the method described by Logan et al. (*19*). Time–activity curves for each ROI of the brain were calculated as becquerels per milliliter or SUV. Using the time–activity curves of the brain tissues and the metabolite-corrected time–activity curve of plasma, the DV for ^{11}C-MPDX was evaluated. Equation 1 describes the concept of the Logan plot in which integrals of the elapsed-time time–activity curve and the plasma time–activity curve normalized by the elapsed-time time–activity curve have a linear relationship and its gradient derives a total DV:

$$\frac{\int_0^t ROI(t')dt'}{ROI(t)} = DV\frac{\int_0^t Cp(t')dt'}{ROI(t)} + int, \qquad \text{Eq. 1}$$

where Cp is activity in plasma, t is elapsed time, and int is integral. A Logan plot was applied to every voxel to make a parametric image on the DV. First, the integrated values were calculated using trapezoidal integration, and Logan plots were formed with an integrated plasma time–activity curve. Then, regression lines were estimated using the plots between 10 and 40 min after ^{11}C-MPDX injection. An estimated gradient means total DV, and an image of the DV can be obtained.

RESULTS

Figure 2 shows the time–activity curves of whole blood and plasma after injection of ^{11}C-MPDX. The SUVs of blood and plasma decreased rapidly for the first 10 min after injection and then decreased gradually. A discrepancy between 2 levels was observed on and after 10 min. The level of blood was slightly higher than that of plasma. Labeled metabolites of ^{11}C-MPDX in plasma were analyzed by HPLC. Three polar metabolites (reten-

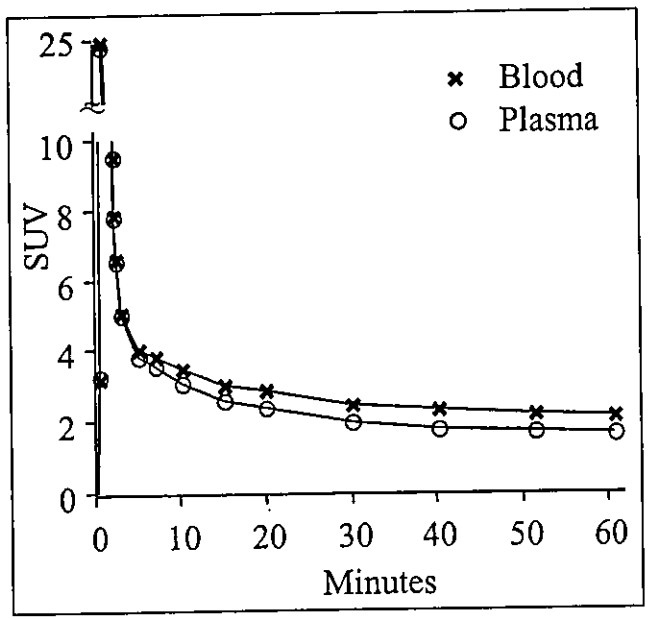

FIGURE 2. Time–activity curves in blood and plasma after injection of ^{11}C-MPDX. Data represent means of 5 subjects. SUVs of blood and plasma decreased rapidly for first 10 min after injection. SUV of blood was slightly higher than that of plasma.

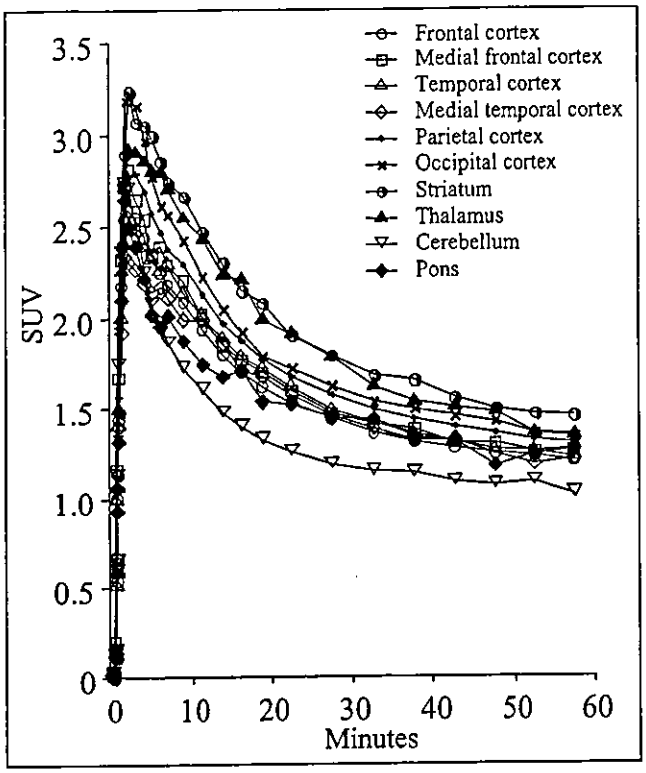

FIGURE 3. Time–activity curves in each region in brain after injection of ^{11}C-MPDX. Data represent means of 5 subjects. Uptake of ^{11}C-MPDX in each region was high, followed by rapid decrease for first 15 min. SUV was relatively high in striatum and thalamus and low in cerebellum.

tion times: 1.8, 3.2, and 4.3 min) were found in addition to ^{11}C-MPDX (retention time: 6.3 min). The unchanged form of ^{11}C-MPDX in plasma was 98.5% ± 0.64% at 3 min, 88.8% ± 2.85% at 10 min, 82.8% ± 5.38% at 20 min, 82.2% ± 8.28% at 30 min, 77.1% ± 5.38% at 40 min, and 74.9% ± 5.00% at 60 min.

Figure 3 shows the time–activity curves of each brain region after injection of ^{11}C-MPDX. ^{11}C-MPDX was taken at high levels in all regions investigated, and the uptake reached a peak at 2–2.5 min after injection, followed by a rapid decrease for the first 15 min. Approximately 6% of the total injected ^{11}C-MPDX was taken up in the brain at 2–2.5 min. The clearance patterns differed slightly among each region. The SUV was relatively high in the striatum and thalamus and low in the cerebellum.

Figure 4 shows the brain MRI and PET parametric images in a typical case. The distribution pattern of ^{11}C-MPDX was discretely different from that of rCBF. The binding of ^{11}C-MPDX was very low in the cerebellum and high in the striatum and thalamus, where the rCBF was relatively lower.

Table 1 summarizes the DV of ^{11}C-MPDX and rCBF. A typical Logan plot was shown in Figure 5. The DV was large in the striatum and thalamus, moderate in 6 cortical regions and the pons, and small in the cerebellum. The DV pattern of ^{11}C-MPDX in the brain was different from the rCBF pattern. The rCBF was low in the temporal and medial frontal cortices and pons.

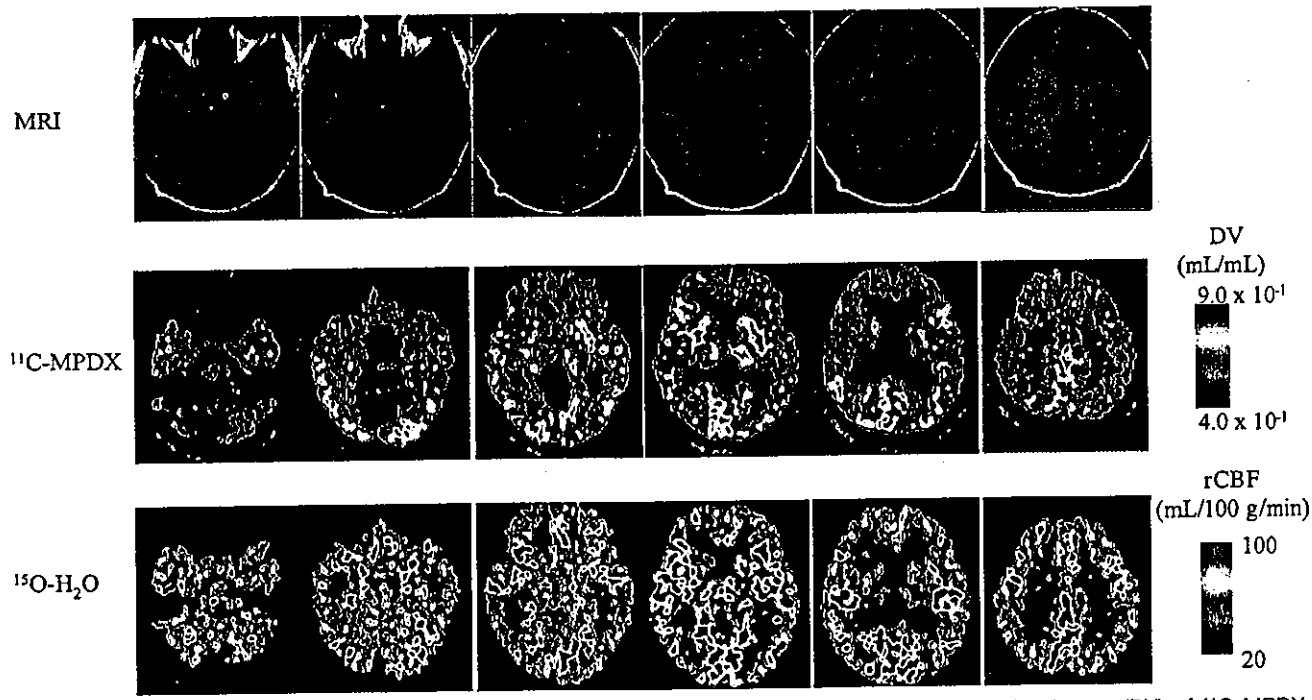

FIGURE 4. Brain MRI and PET parametric images in typical case. (Top) MRI. (Middle) Distribution image (DV) of ^{11}C-MPDX. (Bottom) rCBF with ^{15}O-H_2O. DV of ^{11}C-MPDX was low in cerebellum and high in striatum and thalamus, where rCBF was relatively lower.

TABLE 1
DV of ^{11}C-MPDX and rCBF in Brain Regions of Young Healthy Subjects

Brain region	DV (mL/mL)	rCBF (mL/100 g/min)
Frontal cortex	0.69 ± 0.17	59.9 ± 14.7
Medial frontal cortex	0.70 ± 0.19	65.8 ± 16.8
Temporal cortex	0.70 ± 0.19	53.9 ± 11.4
Medial temporal cortex	0.68 ± 0.18	56.3 ± 13.1
Parietal cortex	0.75 ± 0.18	65.9 ± 18.6
Occipital cortex	0.78 ± 0.21	72.4 ± 20.5
Striatum	0.84 ± 0.23	71.8 ± 23.6
Thalamus	0.81 ± 0.21	72.9 ± 23.5
Cerebellum	0.58 ± 0.14	72.0 ± 23.1
Pons	0.67 ± 0.18	60.4 ± 15.2

Data represent mean ± SD (n = 5).

DISCUSSION

Following the preclinical studies on the mapping of adenosine A_1 receptors in the brain of cats and monkeys by ^{11}C-MPDX PET (*1–15*), we performed a clinical study on ^{11}C-MPDX PET and demonstrated the potential of ^{11}C-MPDX as a radioligand for mapping adenosine A_1 receptors in the human brain (*9*). In the present study, we quantitatively evaluated the binding of ^{11}C-MPDX in the brain of healthy subjects.

In the literature, the adenosine A_1 receptors are rich in the hippocampus, cerebral cortex, thalamic nuclei, and basal ganglia of the postmortem human brain (*16,20,21*). In the cerebral cortex, the adenosine A_1 receptors were rich in primary visual cortex layer III in the occipital cortex and superficial and intermediate layers in the parietal cortex. On the other hand, the density was relatively low in the frontal, temporal, and cingulate cortices. In the present PET study, the binding of ^{11}C-MPDX evaluated quantitatively as the DV was relatively higher in the striatum and thalamus among the brain regions investigated and lower in the cerebellum. In the cerebral cortex, the DV was relatively larger in the occipital and parietal cortices and smaller in the frontal and temporal cortices. The DV pattern of ^{11}C-MPDX in vivo was consistent with that of the A_1 receptor in vitro represented in previous reports (*20–24*), demonstrating that ^{11}C-MPDX is a suitable radioligand for mapping adenosine A_1 receptors.

In the present study, we did not directly certify the specific binding of ^{11}C-MPDX to the adenosine A_1 receptors by blocking studies. However, we previously confirmed the A_1 receptor-specific binding of ^{11}C-MPDX in animals. Coinjection of unlabeled MPDX or A_1-selective KF15372 significantly blocked the brain uptake in mice, rats, and cats (*10–13*). In a PET study with cats, the reversible binding of ^{11}C-MPDX was clearly demonstrated after treatment with A_1-selective 8-cyclopentyl-1,3-dipropylxanthine (DPCPX) (*13*). In the cat and monkey brains, the regional distribution pattern of ^{11}C-MPDX was similar to that of its analog ^{11}C-KF15372 (*13,14*), for which the receptor-specific binding was directly confirmed in the monkey brain (*11*). Furthermore, alteration of ^{11}C-MPDX binding was observed using ex vivo autoradiography in the rat brain treated by monocular enucleation (*12*) and was observed using PET in the cat brain with cerebral ischemic insult (*15*). On the basis of these studies, for the quantitative analysis for ^{11}C-MPDX binding in the human brain, we used Logan plot analysis in the present study because it provides relatively stable results compared with the results of kinetic analysis using a 2- or 3-compartment model.

The DV of ^{11}C-MPDX was relatively smaller in the medial temporal cortex including the hippocampus. In postmortem brain studies, the density of adenosine A_1 receptor binding sites was heterogeneous, and the density was high in the stratum radiatum/pyramidale of CA1 but low in the stratum moleculare of CA1 and the granule cell layer of the dendate gyrus hilus (*20,21*). In ^{11}C-MPDX PET, the DV values in these ROIs were assessed as the means of high and

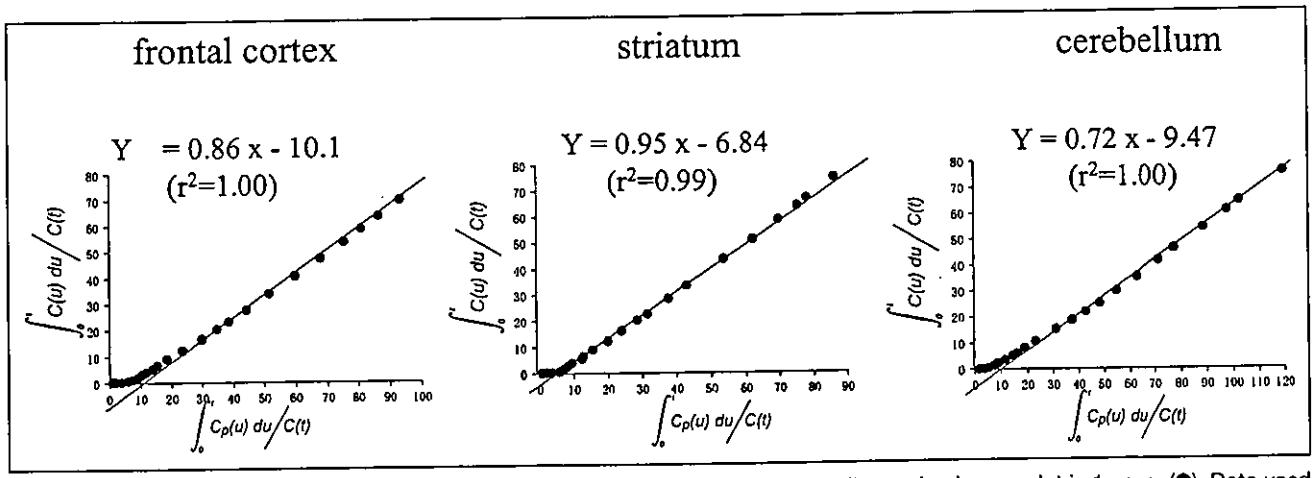

FIGURE 5. Graphical analysis of ^{11}C-MPDX in frontal cortex, striatum, and cerebellum using Logan plot in 1 case. (●), Data used for linear regression analysis. Slopes of fits represent DVs. C = activity in tissue; $Cp(t)$ = activity in plasma; t = elapsed time.

low densities of the binding sites, which resulted in the apparent discrepancy between the in vitro findings and ^{11}C-MPDX PET in the medial temporal cortex. The partial-volume effect based on the spatial resolution may be the other reason why the DV in the medial temporal cortex was relatively small.

We performed successively 2 PET scans with ^{15}O-H_2O and ^{11}C-MPDX in each subject to verify the influence from rCBF. As shown in Figure 4 and Table 1, the DV pattern was distinctly different from the rCBF pattern. The DV was large in the striatum and thalamus and small in the cerebellum showing a high rCBF. Together with the finding that the DV pattern was consistent with the in vitro receptor distribution pattern in the described postmortem studies (*20,21*), we concluded that the DV calculated by Logan plot analysis was a stable and sufficient method to estimate the binding of ^{11}C-MPDX to adenosine A_1 receptors.

As shown in the time–activity curves of whole blood and plasma (Fig. 2), the radioactivity level in blood was slightly higher than that of plasma. The finding suggests the presence of binding sites or an unknown uptake mechanism for ^{11}C-MPDX in blood cells. With regard to the peripheral metabolism of the tracer, we found that ^{11}C-MPDX was relatively stable in our human subjects compared with the metabolism in experimental animals. The unchanged form of ^{11}C-MPDX in human plasma was 75% of the total radioactivity at 60 min after injection, whereas the corresponding figures were 22%–27% at 30 min in rats (*10*), 6.5% at 60 min in cats (*13*), and 41% at 60 min in monkeys (*15*).

Recently, Bauer et al. also successfully performed imaging of adenosine A_1 receptors in the human brain by PET using a similar radioligand, ^{18}F-CPFPX (*16*). They also evaluated the binding of ^{18}F-CPFPX as the DV. The distribution pattern of ^{11}C-MPDX was consistent with that of ^{18}F-CPFPX. However, for the peripheral metabolism, ^{11}C-MPDX was much more stable than ^{18}F-CPFPX. The unchanged form of ^{18}F-CPFPX in the plasma decreased rapidly <25% after 10 min after injection, whereas the percentages of unchanged ^{11}C-MPDX in the plasma remained high during the 60-min PET scan: 89% at 10 min and 75% at 60 min after injection. Although ^{11}C-MPDX (inhibition constant [K_i] = 4.2 nmol/L for the rat forebrain membrane) (*10*) has a slightly lower affinity for A_1 receptors than ^{18}F-CPFPX (K_i = 1.26 nmol/L for the cloned human A_1 receptors) (*25*), the in vivo stability of ^{11}C-MPDX is the advantage of the continuous input function for the kinetic analysis. On the other hand, ^{18}F-CPFPX has practical advantages: ^{18}F provides a slightly better resolution of the images and its longer half-life of is more suitable to handle in clinical use compared with ^{11}C-labeled tracers.

Coexpression of and functional interactions between adenosine A_1 and dopamine D_1 receptors in the striatum of rat and rabbit have been reported (*26*). The similarity in distribution of these receptors types suggests that such an interaction might also occur in the human brain. They are important for cholinergic neurotransmission. Adenosine plays an important role in sleep, and adenosine receptor antagonists such as caffeine promote wakefulness and disrupt normal sleep (*4,27*). Studies on the postmortem human brain reported a reduced density of adenosine A_1 receptors in the hippocampus of patients with Alzheimer's disease (*28–30*). The anticonvulsant effects of adenosine appear to be mediated primarily by A_1 receptors (*31,32*). Carter et al. reported that arousal detected by electroencephalography after caffeine ingestion might be due to increased cholinergic activity (*33*). Angelatou et al. detected a significant increase in adenosine A_1 receptor binding in the neocortex obtained from patients with temporal lobe epilepsy (*34*), whereas Glass et al. found that the adenosine A_1 receptors were reduced in epileptic temporal cortex in temporal lobes removed from patients with complex partial seizures (*35*). The ^{11}C-MPDX PET is of great interest in establishing the diagnosis of patients with somnipathy, epilepsy, Alzheimer's disease, and other neurologic and psychiatric diseases and understanding the pathogenesis and treatment effect.

CONCLUSION

^{11}C-MPDX was widely but discretely distributed with different concentrations in the brain. The binding of ^{11}C-MPDX was high in the striatum and thalamus, intermediate in the cerebral cortices, and low in the cerebellum. The distribution pattern of ^{11}C-MPDX was consistent with that of adenosine A_1 receptors in vitro but discretely different from that of rCBF. The ^{11}C-MPDX PET has the potential for mapping adenosine A_1 receptors in the human brain. ^{11}C-MPDX PET is useful for mapping adenosine A_1 receptors in the human brain.

REFERENCES

1. Collis MG, Hourani SMO. Adenosine receptor subtypes. *Trends Pharmacol Sci.* 1993;14:360–366.
2. Fredholm BB, Abbracchio MP, Burnstock G, et al. Nomenclature and classification of purinoceptors. *Pharmacol Rev.* 1994;46:143–156.
3. Haas HL, Selbach O. Functions of neuronal adenosine receptors. *Naunyn Schmiedebergs Arch Pharmacol.* 2000;362:375–381.
4. Dunwiddie TV, Masino SA. The role and regulation of adenosine in the central nervous system. *Annu Rev Neurosci.* 2001;24:31–55.
5. von Lubitz DK. Adenosine in the treatment of stroke: yes, maybe, or absolutely not? *Expert Opin Investig Drugs.* 2001;10:619–632.
6. Yacoubi ME, Costentin J, Vaugeois JM. Adenosine A_{2A} receptors and depression. *Neurology.* 2003;61:S82–S87.
7. Suzuki F, Ishiwata K. Selective adenosine antagonists for mapping central nervous system adenosine receptors with positron emission tomography: carbon-11 labeled KF15372 (A_1) and KF17837 (A_{2A}). *Drug Develop Res.* 1998;45:312–323.
8. Ishiwata K, Shimada J, Ishii K, Suzuki F. Assessment of the adenosine A_{2A} receptors with PET as a new diagnostic tool for neurological disorders. *Drugs Fut.* 2002;27:569–576.
9. Fukumitsu N, Ishii K, Kimura Y, et al. Imaging of adenosine A_1 receptors in the human brain by positron emission tomography with [^{11}C]MPDX. *Ann Nucl Med.* 2003;17:511–515.
10. Noguchi J, Ishiwata K, Furuta R, et al. Evaluation of carbon-11 labeled KF15372 and its ethyl and methyl derivatives as a potential CNS adenosine A_1 receptor ligand. *Nucl Med Biol.* 1997;24:53–59.
11. Wakabayashi S, Nariai T, Ishiwata, et al. A PET study of adenosine A1 receptor in anesthetized monkey brain. *Nucl Med Biol.* 2000;27:401–406.
12. Kiyosawa M, Ishiwata K, Noguchi J, et al. Neuroreceptor bindings and synaptic

activity in visual system of monocularly enucleated rat. *Jpn J Ophthalmol.* 2001;45:264–269.
13. Shimada Y, Ishiwata K, Kiyosawa M, et al. Mapping adenosine A_1 receptors in the cat brain by positron emission tomography with [^{11}C]MPDX. *Nucl Med Biol.* 2002;29:29–37.
14. Ishiwata K, Nariai T, Kimura Y, et al. Preclinical studies on [^{11}C]MPDX for mapping adenosine A_1 receptors by positron emission tomography. *Ann Nucl Med.* 2002;16:377–382.
15. Nariai T, Shimada Y, Ishiwata K, et al. PET imaging of adenosine A_1 receptors with ^{11}C-MPDX as an indicator of severe cerebral ischemic insult. *J Nucl Med.* 2003;44:1839–1844.
16. Bauer A, Holschbach MH, Meyer PT, et al. In vivo imaging of adenosine A_1 receptors in the human brain with [^{18}F]CPFPX and positron emission tomography. *Neuroimage.* 2003;19:1760–1769.
17. Ardekani BA, Braun M, Hutton BF, Kanno I, Iida H. A fully automatic multimodality image registration algorithm. *J Comput Assist Tomogr.* 1995;19:615–623.
18. Herscovitch P, Markham J, Raichle ME. Brain blood flow measured with intravenous $H_2{}^{15}O$. I. Theory and error analysis. *J Nucl Med.* 1983;24:782–789.
19. Logan J, Fowler JS, Volkow ND, et al. Graphical analysis of reversible radioligand binding from time-activity measurements applied to [N-^{11}C-methyl]-(-)-cocaine PET studies in human subjects. *J Cereb Blood Flow Metab.* 1990;10:740–747.
20. Svenningsson P, Hall H, Sedvall G, Fredholm BB. Distribution of adenosine receptors in the postmortem human brain: an extended autoradiographic study. *Synapse.* 1997;27:322–335.
21. Fastbom J, Pazos A, Probst A, Palacios JM. Adenosine A_1 receptors in the human brain: a quantitative autoradiographic study. *Neuroscience.* 1987;22:827–839.
22. Lewis ME, Patel J, Moon ES, Marangos PJ. Autoradiographic visualization of rat brain adenosine receptors using N^6-cyclohexyl[^{3}H]adenosine. *Eur J Pharmacol.* 1981;73:109–110.
23. Goodman RR, Snyder SH. Autoradiographic localization of adenosine receptors in rat brain using [^{3}H]cyclohexyladenosine. *J Neurosci.* 1982;2:1230–1241.
24. Fastbom J, Pazos A, Palacios JM. The distribution of adenosine A1 receptors and 5′-nucleotidase in the brain of some commonly used experimental animals. *Neuroscience.* 1987;22:813–826.
25. Holschbach MH, Olsson RA, Bier D, et al. Synthesis and evaluation of no-carrier-added 8-cyclopentyl-3-(3-[^{18}F]fluoropropyl)-1-propylxanthine ([^{18}F]CPFPX): a potent and selective A_1-adenosine receptor antagonist for in vivo imaging. *J Med Chem.* 2002;45:5150–5156.
26. Ferre S, O'Connor WT, Svenningson P, et al. Dopamine D_1 receptor-mediated facilitation of GABAergic neurotransmission in the rat strioentopeduncular pathway and its modulation by adenosine A_1 receptor-mediated mechanisms. *Eur J Neurosci.* 1996;8:1545–1553.
27. Radulovadei M. Role of adenosine in sleep in rats. *Rev Clin Basic Pharmacol.* 1985;5:327–339.
28. Jansen K, Faull RLM, Dragunow M, Synek BJL. Alzheimer's disease: changes in hippocampal *N*-methyl-D-aspartate, quisqualate, neurotensin, adenosine, benzodiazepine, serotonin and opioid receptors—an autoradiographic study. *Neuroscience.* 1990;39:613–627.
29. Ulas J, Brunner LC, Nguyen L, Cotman CW. Reduced density of adenosine A1 receptors and preserved coupling of adenosine A1 receptors to G proteins in Alzheimer hippocampus: a quantitative autoradiographic study. *Neuroscience.* 1993;52:843–854.
30. Deckert J, Abel F, Kunig G, et al. Loss of human hippocampal adenosine A1 receptors in dementia: evidence for lack of specificity. *Neurosci Lett.* 1998;244:1–4.
31. Murray TF, Franklin PH, Zhang G, Tripp E. A_1 adenosine receptors express seizure-suppressant activity in the rat prepiriform cortex. *Epilepsy Res Suppl.* 1992;8:255–261.
32. Zhang G, Franklin PH, Murray TF. Activation of adenosine A1 receptors underlies anticonvulsant effect of CGS21680. *Eur J Pharmacol.* 1994;255:239–243.
33. Carter AJ, O'Connor WT, Carter MJ, Ungerstedt U. Caffeine enhances acetylcholine release in the hippocampus in vivo by a selective interaction with adenosine A1 receptors. *J Pharmacol Exp Ther.* 1995;273:637–642.
34. Angelatou F, Pagonopoulou O, Maraziotis T, et al. Upregulation of A1 adenosine receptors in human temporal lobe epilepsy: a quantitative autoradiographic study. *Neurosci Lett.* 1993;163:11–14.
35. Glass M, Faull RL, Bullock JY, et al. Loss of A1 adenosine receptors in human temporal lobe epilepsy. *Brain Res.* 1996;710:56–68.